Turkish Journal of Electrical Engineering & Computer Sciences

http://journals.tubitak.gov.tr/elektrik/

Research Article

Turk J Elec Eng & Comp Sci
(2022) 30: 1097 – 1114

doi:10.3906/elk-2108-201

Identification of gain and phase margins based robust stability regions for a time-delayed micro-grid system including fractional-order controller in presence of renewable power generation

Hakan GÜNDÜZ[1], **Şahin SÖNMEZ**[2,*], **Saffet AYASUN**[3]

[1]Department of Property Protection and Security, Boyabat Vocational High School, Sinop University, Sinop, Turkey

[2]Department of Electronics and Automation, Yesilyurt Vocational High School, Malatya Turgut Özal University,Malatya, Turkey

[3]Department of Electrical and Electronics Engineering,Faculty of Engineering, Gazi University,Ankara, Turkey

Received: 31.08.2021 • **Accepted/Published Online:** 17.01.2022 • **Final Version:** 21.03.2022

Abstract: This study examines the gain and phase margins (GPMs) based robust stability margins in the parameter space of fractional order proportional-integral (FOPI) controller for a micro-grid (MG) system with communication time delays. Fluctuations in renewable energy sources (RESs), uncertainties in parameters of system components and communication delays could adversely affect the dynamical analysis and frequency stability of the MG system. Such a MG system has an interval characteristic due to the parametric variations and the interval transfer functions defined by Kharitonov's theorem, which presents a solution for checking of robust stability. Therefore, this study addresses the robust stability regions containing a set of robust FOPI controller gains for all possible transfer functions of the MG system by a simple graphical method working in controller parameter space. In this way, the impact of fractional order degree of integral controller on the robust stability regions is exhaustively examined by the graphical method. Additionally, robust performance of the interval MG system in terms of design specifications including GPMs is analyzed, and the effect of GPMs on the robust regions is investigated by the graphical method. Results indicate that GPM parameters provide the desirable performances for the MG and fractional order of integral controller considerably increases the robustness of the stability margin of the MG when compared with the integer order PI controller.

Key words: Micro-grids, gain and phase margins, robust stability region, fractional-order controller

1. Introduction

Together with development of renewable energy technologies, the integration of distributed generations (DGs) such as photovoltaic (PV) systems and wind turbine (WT) into power systems have been gradually increased to reduce the detrimental effects of traditional power generations on the environmental and economic concerns [1, 2]. The equipment such as micro-turbine (MT), fuel cell (FC) - electrolyzer (ES), communication infrastructures, and various load groups along with renewable energy sources (RESs) constitute the main components of a small-scale micro-grid (MG) [3–5]. MGs have following important advantages in terms of stable and economic operation of power systems: (i) to meet regional power generation needs, (ii) to improve the security and reliability of power systems, (iv) to decrease the transmission cost at distribution level and to economically

*Correspondence: ssonmeztr@gmail.com

operate the generation units during peak time [1, 3]. Since MGs are a small part of power systems, they could be operated in grid connected mode and islanded mode [5]. In grid connected mode, MGs become more powerful and stable than the islanded mode because of their interconnection with the main grid. While in the islanded mode, MGs transfer power to/from storage units for keeping the active and reactive power balance. However, the islanded MGs cannot tolerate large disturbances like variations in RESs and sudden power fluctuations [6]. Besides, [6, 7] report that high level integration of RESs into MGs leads to the lack of inertia, which is required to increase the reliability and security of the system. These challenges could degrade power quality of the MGs and even leads to instability.

MGs are responsible for keeping the stable frequency profile as an indication of system reliability and security during load disturbance events. For this objective, a MG central controller (MGCC), which is equipped with open communication networks [5] is employed to keep the system frequency and voltage in acceptable nominal values. The MGCC with communication networks could usually mitigate the frequency deviations by implementing the traditional load frequency control (LFC) based on proportional-integral (PI) or proportional integral-derivative (PID) [8]. The main goals of MGCC are to receive various measurements from each DG, to transmit the control information to local primary controllers via communication channels and to adjust the real power set-points of each DG for economic operation of MGs [3, 9–11]. Due to the utilization of the communication networks, the time delay issue of the MG LFC systems is inevitable. The time delay term as an exponential expression is introduced to the secondary control loop of MG system. The networked-induced time delays for the information transmission could be random or unknown depending upon considerations such as inner mechanism of communication channels, network load and communication medium [5, 12, 13]. Even though MGCC needs support from the communication networks to maintain the stable operation of system, the network-induced communication delays deteriorate dynamic performance and may destabilize the system [5, 9] When the communication requirement of the LFC system exceeds the delay margin value known as maximum allowable delay, the system frequency deviation and dynamic performance exhibit an unstable behaviour [3, 5, 11].

Uncertainties in communication time delays, external disturbances (wind, solar and load uncertainties) and varying system parameters are significant challenges for robust frequency stability of MG systems. In the literature, sliding mode control, H_∞ and μ synthesis controls were implemented to improve the robust frequency stabilization of MGs having parametric uncertainties [14, 15]. Also, the robust stability of frequency and voltage for the MGs with parametric uncertainties was guaranteed by finite-time secondary control method [16]. For the design of robust controller parameters against the uncertainties of system parameters, many studies have proposed Kharitonov's theorem based only on four polynomials for checking the stability of interval plants whose parameters are varied in a prescribed interval [17–19]. The study reported in [17] utilized this theorem to tune the integer order PI (IOPI) controllers for robust LFC design of the MG with/without time delay. This technique was efficiently implemented to maintain the robust frequency stability and to obtain a set of robust controller parameters for conventional power systems with IOPI [18, 19] and fractional order PI (FOPI) controller [20–22] and to design the controller parameters for robust voltage stability of islanded MG systems [23]. Finally, the study reported in [24] proposed an adaptive robust control model to coordinate multi-MGs control system. Stability evaluation methods considering uncertainty, such as various perturbations and communication failure, were proposed to analyze delay-independent system using Lyapunov stability without delay. In order to eliminate the adverse effects of delay caused by wide-area measurement, an active disturbance rejection

stabilizer is designed.

Although IOPI controllers have been efficiently used for the delay-dependent stability analysis and robust system analysis due to their practicable structure and simplicity, the FOPI controllers offer more flexibility and more degree of freedom to improve the system performance towards parametric uncertainty and external disturbances [20–22]. The outstanding performance of FO controllers has attracted the attention of researchers to implement the controller type in MG frequency control systems. Many research studies optimized the FOPI/FOPID parameters using various optimization techniques and investigated the robustness and stability analysis of MG LFC system under load perturbations, variations in renewable energy sources, and various failures [25, 26]. Additionally, the study reported in [27] proposed the enhanced fractional order fuzzy PID controller for frequency regulation of an AC micro-grid. This study conducted the sensitivity analysis to validate the robustness of the proposed controller parameters under variations parameters and communication delay, and then the accuracy of practical feasibility of the proposed method and obtained results was shown by the real-time simulator. Another study [28] carried out the type-2 fuzzy fractional-order PD-PI controller for frequency regulation of the MG system, and the robustness of proposed method against several uncertainties was investigated by real-time simulator. Considering the impact of FOPI controller on the robust stability for the MG working in uncertain environment, this paper investigates the robust stability regions of the MG system including both FOPI and communication time delay using Kharitonov's theorem, emphasizing first contributions of this paper. For this, all possible characteristic polynomials described by Kharitonov theorem for the interval MG system are first obtained. Then, a simple graphical method, well known as stability boundary locus (SBL) method, is applied to all obtained possible characteristic equations for the interval MG system. By equating the imaginary and real parts of the characteristic polynomial of the MG system to zero, the procedure easily identifies all stabilizing PI controller parameters in the parameters plane of PI controller [29, 30]. Consequently, the robust stability region in PI controller plane for the interval system could be extracted from the intersection of the all possible stability regions identified by SBL method. The method was efficiently implemented to investigate the stability regions of a time-delayed MG with gain and phase margins (GPMs) [3], a time-delayed MG enhanced by the electric vehicle [31], a conventional power systems with time delay [32–34], large wind turbine systems with FOPI controller [35] and a time-delayed MG including FOPI [36, 37]. The robust stability analysis of the fractional order/integer order interval systems with parametric uncertainties using Kharitonov theorem have been a topic of interest of researchers. [20] designed the robust FOPID controller gains by using sixteen Kharitonov polynomials for LFC system with reheated turbine where the four Kharitonov polynomials for both numerator and denominator polynomials of the open loop transfer function are defined. In the same study, eight Kharitonov polynomials for LFC system with nonreheated turbine is employed to obtain the robust stability region. [21] defined four Kharitonov polynomials for both numerator and denominator polynomials of the open loop transfer function of the each frequency control area by decoupling the two-area LFC system with uncertainty parameters, resulting in total sixteen Kharitonov polynomials. Moreover, [38] proposed the incorporation of the Kharitonov and Edge theorems for the robust stability analysis of fractional order interval systems with fractional order controller. The proposed incorporation was applied to the different fractional order interval systems with parametric uncertainty and was presented the important results.

From a practical perspective, not only robust stability regions but also frequency domain specifications such as gain margin (GM) and phase margin (PM) providing robust performance of the MG must also be taken into account along with robust stability margins to achieve all admissible robust PI controller gains. The consideration of GM and PM also enables us to choose flexible PI controller coefficients for practical

frequency responses regarding frequency domain design specifications such as shorter settling time, overshoot, and minimum deviation, which is the second main contribution of the study. In order to identify the user-defined GPM specifications, a gain - phase margin tester (GPMT) is inserted to forward part of controller [39]. Focusing on GPM based robust stability regions of the MG with FOPI controller, the significant contributions of this study are listed as follows:

- Robust stability regions of MG system including FOPI controller under parametric uncertainties are computed by SBL method and Kharitonov's theorem.
- The impact of fractional order of integral controller on the robust stability regions is exhaustively investigated. The results indicate that FOPI controller significantly improves the robust stability regions and, thus, increases robustness margin towards gain variations of the FC-ES and MT systems
- The GPM based robust FOPI controller parameters against parametric variations of MG system are obtained to analyze the effect of GPMs on the robust regions.
- Finally, performances of robust stability regions are investigated by time domain simulations during external disturbances like various loads, wind and solar power fluctuations [40]. The simulation results show that selected controller gains from GPM based robust stability regions improve dynamic performance of system, and FOPI controller exhibits a more attractive performance as compared with IOPI controller.

The remaining article is structured as following: Section II presents the description and dynamical model of the MG system including time delays and FOPI controller. Section III provides the implementation of Kharitonov's theorem and SBL method. Section IV gives FOPI and GPMs based robust stability regions and simulation studies while Section V concludes the paper.

2. Description and dynamical modelling of the MG system studied

Modern MGs are usually known as cyber physical energy systems (CPES) which perform various control functions and coordinate all DG units via communication networks. While physical layers of CPES include the dispersed power networks such as WT, PV, MT, and FC, cyber layers contain local and centralized controllers equipped with communication networks used to manage and to monitor the security and reliability of the system [41]. Accordingly, Figure 1 represents schematic diagram of a small-scale MG that is composed of WT, PV, FC, MT, ES, MGCC, and communication networks. Here, a gas based MT system is installed to supply the base load and its power is controlled by local controller and MGCC. Additionally, a FC to provide the power support to MT during peak times is installed. Due to intermittent nature of solar and wind powers, the small scale MG system faces with some stability challenges in keeping the frequency stabilization [6, 7]. The instable feature of the wind and solar sources leads to sudden real power unbalance resulting in large frequency fluctuations[3, 11]. Although the MT system is placed to balance the sudden power changes owing to its dynamical capability, it could not alleviate fast frequency fluctuations due to its slow dynamic behavior. For this reason, the ES is used to rapidly response to the power fluctuations arisen from wind and solar generations and to avoid larger frequency deviation [2]. For this purpose, the ES as the real power observer is employed to enhance the dynamical stability of MG. The two key advantages of ES are as follows: i) it is to provide the load controllable operation for the MG system, ii) it is to produce hydrogen using power generated in WT and PV, and, hence, the fuel stored in hydrogen tank is converted to electrical power by FC [2]. Therefore,

the power consumption of ES depending upon frequency error of the system is adjusted by MGCC. Installed capacities of the generation units and local loads are considered as WT of 100 kW, PV of 25 kW, FC of 5 kW, ES of 70 kW, MT of 100 kW and load group of 80 kW [2]. The system base is 100kW. CPES has emerged as a significant tool to improve the capability of computational, communication and control of MGs. However, major challenges such as cyber-attacks, false data injections, communication network failures, any failures in the physical components could considerably affect the security and reliability of CPES [41].

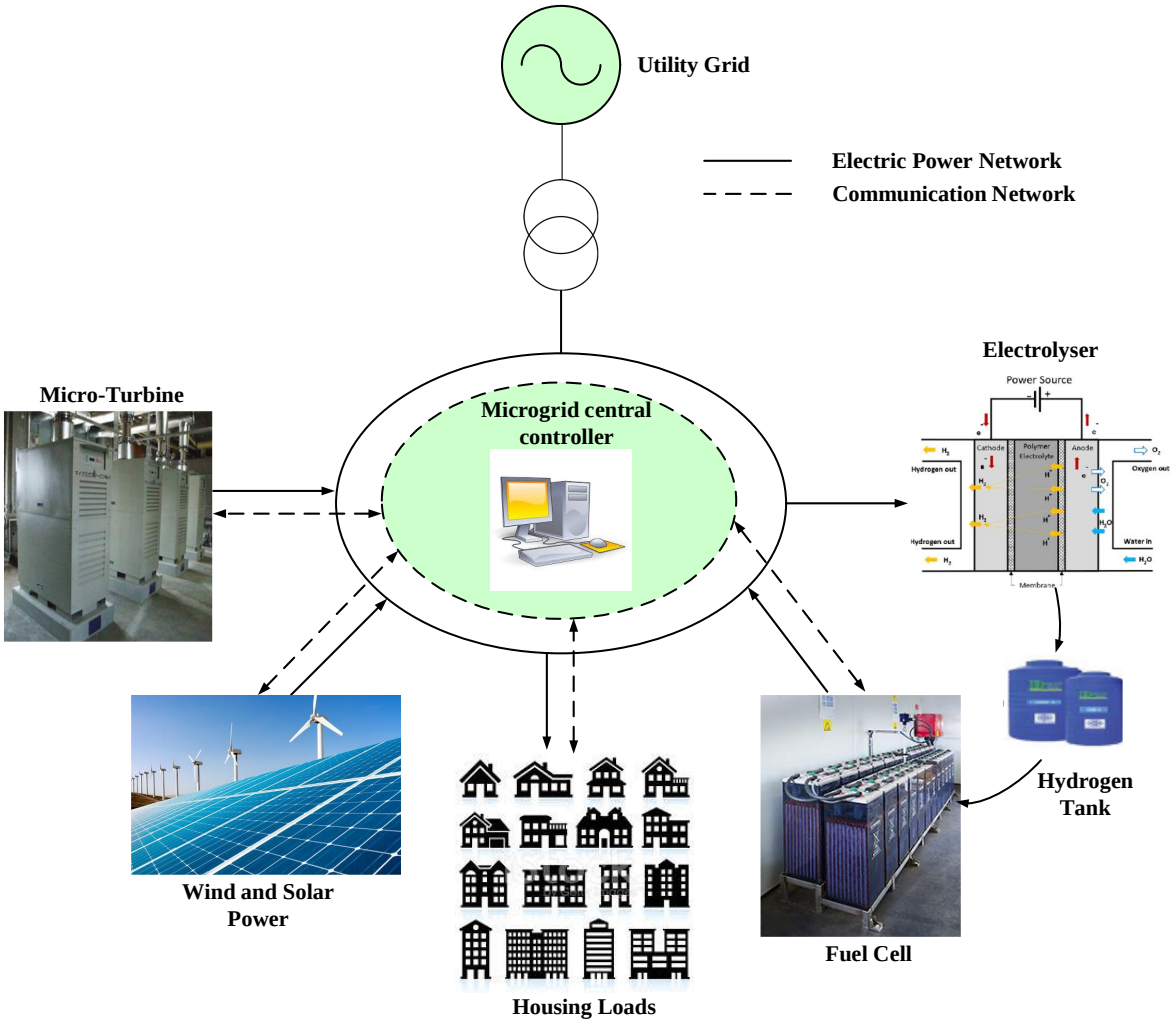

Figure 1. Schematic diagram of MG system.

The dynamics of MG-LFC system without/with time delays are usually expressed by a set of differential-algebraic and/or nonlinear differential equations [42]. When the MG-LFC system is subjected to a small disturbance, linearizing the nonlinear equations around an equilibrium point, linearized state-space equations of the system is computed. The linearized models are sufficient to evaluate the steady-state or small-signal stability of the MG-LFC around a stable operating point [41]. Therefore, in order to investigate the stability analysis and dynamic behavior of the CPES, linearized first order transfer functions for each component of a MG system as shown in Figure 2 are used. In this model, frequency deviation ($\Delta f(s)$) and control signals

($U_c(s)$) represented by dashed line show cyber signals of the MG, whereas MT, FC, ES, loads represent the physical components of MG system. Primary control side is composed of ES, FC, and MT model consisting of a local controller and a droop characteristic control. The function of droop control mechanism is to make a proper set point for meeting the active and reactive power demand and, thus, to manage the coordination among all DGs. Also, a PI based local controller is utilized to control power sharing among DGs [1]. Simplified transfer functions of MT and local control unit are given as follows:

$$G_{MT}(s) = \frac{\Delta f}{\Delta P_T} = \frac{1}{Ms + D} \tag{1}$$

$$G_{LC}(s) = K_{PL} + \frac{K_{IL}}{s} \tag{2}$$

Referring to the charging/discharging of a battery energy storage device [2], the FC and ES are expressed by a first-order transfer function as follows:

$$G_{FC}(s) = \frac{\Delta P_{FC}}{\Delta f} = \frac{K_{FC}}{1 + T_{FC}s} \tag{3}$$

$$G_{ES}(s) = \frac{\Delta P_{ES}}{\Delta f} = \frac{K_{ES}}{1 + T_{ES}s} \tag{4}$$

In Figure 2, ΔP_{ES}, ΔP_{FC} and ΔP_{MT} represent changes in output power of ES, FC, and MT, respectively. K_{MT}, K_{PL} and K_{IL} represent local controller parameters and drop characteristic of MT. Whereas, K_{ES}, T_{ES}, K_{FC} and T_{FC} denote time constants and gains of the electrolyser and fuel cell, respectively. Also, M and D are inertia and damping constants of the MT, respectively. Here, the FOPI based a MGCC is adopted to secondary control level of MG:

$$G_{CC}(s, \lambda) = K_{PC} + \frac{K_{IC}}{s^{\lambda}} \tag{5}$$

where K_{PC} and K_{IC} are the gains of MGCC PI controller. Also, λ represents fractional order of integral controller and its value could be selected in a range of (0,2) [18]. In this model, total electrical power in the MG system is the algebraic summation of power consumption and generation as follows:

$$\Delta P_T = \Delta P_{FC} + \Delta P_{MT} + \Delta P_{WT} + \Delta P_{PV} - \Delta P_L - \Delta P_{ES} \tag{6}$$

where ΔP_L, ΔP_{PV} and ΔP_{WT} are deviations in load demand (as total of residential and industrial loads), solar power, wind power, respectively. Random power fluctuations in wind and solar powers and load demand are performed by standard deviations dP_L, dP_{WT} and dP_{PV} [3, 43]:

$$\begin{aligned} dP_L &= 0.6\sqrt{P_L} \\ dP_{PV} &= 0.7\sqrt{P_{PV}} \\ dP_{WT} &= 0.8\sqrt{P_{WT}} \end{aligned} \tag{7}$$

The random fluctuations of output power are multipled with corresponding standard deviations and hence the load demand, wind and solar power outputs could be easily simulated in Matlab/Simulink [40]. Finally, τ represents total communication time delays for receiving/transmitting the data between MGCC and DGs. The

delay term is modeled as an exponential transfer function of $e^{-s\tau}$ and assumed to be constant. In order to define the desired frequency specifications, the GPMT as a "virtual compensator" is introduced to the feed forward part in MGCC loop of the MG illustrated in Figure 2 and written as:

$$C(A,\phi) = Ae^{-j\phi} \tag{8}$$

where ϕ and A represent phase margin and gain margin, respectively. In order to compute the robust stability regions and to implement Kharitonov's theorem to the time-delayed MG including FOC, the transfer function $G_P(s)$ of the MG system could be obtained as:

$$G_P(s) = \frac{\Delta f(s)}{\Delta X_C(s)} = \frac{N(s)}{D(s)} = \frac{b_2 s^2 + b_1 s + b_0}{a_3 s^3 + a_2 s^2 + a_1 s + a_0} \tag{9}$$

where $N(s)$ and $D(s)$ are numerator and denominator polynomials of $G_P(s)$, respectively. Coefficients of these polynomials, b_i $(i = 0,1,2)$ and a_i $(i = 0,1,2,3)$ are the constant coefficients in terms of MT and FC-ES system parameters given as (25) in Appendix.

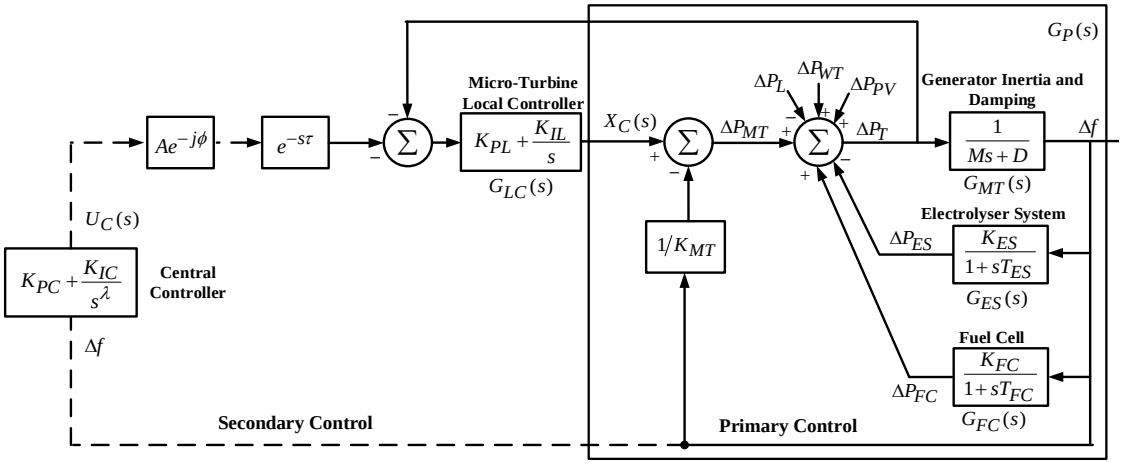

Figure 2. Dynamical model of MG system including FOPI controller.

3. Calculation of the robust stability regions

3.1. Implementation of Kharitonov's theorem

In practical and real power systems, system parametric uncertainty and modelling errors could degrade system performance and lead to instability of the system. Kharitonov's theorem, which is an expansion of Routh–Hurwitz stability theorem is implemented to tackle the robustness concern of system transfer function (9) whose coefficients vary in the prescribed upper and lower limits. The transfer function having perturbed coefficients is described as an interval polynomial. Kharitonov's theorem aims to test and provide robust stability of the system using the interval polynomial that is a set of polynomials forming the uncertain parameters. The theorem uses only four polynomials satisfying conditions of Routh–Hurwitz stability theorem to investigate the robust stability of (9). The four Kharitonov polynomials for both numerator and denominator polynomials of the

interval MG system are expressed as follows:

$$\begin{aligned} N_1(s) &= \underline{b}_0 + \underline{b}_1 s + \bar{b}_2 s^2 \\ N_2(s) &= \underline{b}_0 + \bar{b}_1 s + \bar{b}_2 s^2 \\ N_3(s) &= \bar{b}_0 + \underline{b}_1 s + \underline{b}_2 s^2 \\ N_4(s) &= \bar{b}_0 + \bar{b}_1 s + \underline{b}_2 s^2 \end{aligned} \tag{10}$$

$$\begin{aligned} D_1(s) &= \underline{a}_0 + \underline{a}_1 s + \bar{a}_2 s^2 + \bar{a}_3 s^3 \\ D_2(s) &= \underline{a}_0 + \bar{a}_1 s + \bar{a}_2 s^2 + \underline{a}_3 s^3 \\ D_3(s) &= \bar{a}_0 + \underline{a}_1 s + \underline{a}_2 s^2 + \bar{a}_3 s^3 \\ D_4(s) &= \bar{a}_0 + \bar{a}_1 s + \underline{a}_2 s^2 + \underline{a}_3 s^3 \end{aligned} \tag{11}$$

where $N_k(s)$ and $D_l(s)$ $(k,l = 1,2,3,4)$ are known as vertex polynomials described for the numerator and denominator of the transfer function $G_P(s)$ given in (9). The vertex polynomials proposed by Kharitonov will be used to evaluate system robustness [17, 18]. The coefficients of vertex polynomials $\underline{a}_i \le a_i \le \bar{a}_i$ $\left(\underline{a}_i, \bar{a}_i \neq 0, , i = 0,1,2,3\right)$ and $\underline{b}_i \le b_i \le \bar{b}_i$ $\left(\underline{b}_i, \bar{b}_i \neq 0, , i = 0,1,2\right)$ represent the lower and upper limits of perturbed system parameters of the interval MG. It is to be noted that drop characteristic of MT, FC-ES, system inertia, and damping have the perturbed parameters. The interval coefficients of (10) and (11) showing the variations of system parameters are presented in (26) of Appendix. Considering all combinations of four numerator Kharitonov polynomials ($N_1(s)$ to $N_4(s)$) and four denominator Kharitonov polynomials ($D_1(s)$ to $D_4(s)$), the family of Kharitonov transfer functions are constituted as follows:

$$G_P(s) = \left\{ G_{P_{k,l}}(s) \middle| G_{P_{k,l}}(s) = \frac{N_k(s)}{D_l(s)} k,l = 1,2,3,4 \right\} \tag{12}$$

where k and l notations imply Kharitonov's transfer function corresponding to k^{th} numerator and l^{th} denominator. Therefore, $G_{P_{k,l}}(s)$ represents one of total sixteen Kharitonov transfer functions formed for the interval MG plant as $G_P \in \left\{G_{P_{1,1}}, G_{P_{1,2}}, ..., G_{P_{4,3}}, G_{P_{4,4}}\right\}$. The sixteen transfer functions constitute an interval polynomial family given in (12) and are utilized to obtain the set of Kharitonov characteristic polynomials in controller parameter design of the MG including FOPI. It is said that the interval MG system will be stable if Routh–Hurwitz stable test is satisfied for each of sixteen characteristic equation [17–19]. It should be noted that the studied MG LFC system is an integer order system and only PI controller structure is fractional order. Therefore, the robust stability of an interval system by Kharitonov theorem is typically assessed by using the open loop transfer function model where uncertainty parameters exist [17, 18, 20, 21].

3.2. Identification of stability regions

This section presents the computation of GPM-based stability regions that contain all stabilizing FOPI controller parameters of any transfer function given in (12) for a finite τ. The system characteristic equation including GPM specifications for one of mentioned sixteen transfer functions should be written in the following form:

$$\Delta(s,\lambda,\tau) = P(s,\lambda) + Q(s,\lambda)e^{-(s\tau + j\phi)} = 0 \tag{13}$$

where $P(s,\lambda)$ and $Q(s,\lambda)$ polynomials of the characteristic equation is given as:

$$\begin{aligned} P(s,\lambda) &= p_5 s^{4+\lambda} + p_4 s^{3+\lambda} + p_3 s^{2+\lambda} + p_2 s^{1+\lambda} + p_1 s^{\lambda} \\ Q(s,\lambda) &= q_4 s^{3+\lambda} + q_3 s^{2+\lambda} + q_2 s^{1+\lambda} + q_1 s^{\lambda} + q_0 \end{aligned} \tag{14}$$

where q and p are real coefficients of $Q(s,\lambda)$ and $P(s,\lambda)$ polynomials depending on MG system parameters expressed as (27) in Appendix. It is to be noted from (27) that the coefficients of $Q(s,\lambda)$ polynomial involve the gain margin (A) specification. In order to identify the stability regions, the characteristic polynomial of (13) in terms of FOPI controller parameters (K_{PC}, K_{IC}) is first rearranged for $s = j\omega_c$ with $\omega_c > 0$ is given as follows:

$$\begin{aligned} &\Delta(j\omega_c,\lambda,\tau) = p_5(j\omega_c)^{4+\lambda} + p_4(j\omega_c)^{3+\lambda} + p_3(j\omega_c)^{2+\lambda} + p_2(j\omega_c)^{1+\lambda} + p_1(j\omega_c)^{\lambda} + \\ &K_{PC}\left(q'_4(j\omega_c)^{3+\lambda} + q'_3(j\omega_c)^{2+\lambda} + q'_2(j\omega_c)^{1+\lambda} + q'_1(j\omega_c)^{\lambda}\right)e^{-j(\omega_c\tau+\phi)} + \\ &K_{IC}\left(q''_3(j\omega_c)^{2+\lambda} + q''_2(j\omega_c)^{1+\lambda} + q''_1(j\omega_c)^{\lambda} + q''_0\right)e^{-j(\omega_c\tau+\phi)} = 0 \end{aligned} \tag{15}$$

Note that q' and q'' are coefficients not including (K_{PC} and K_{IC}) controller parameters of $Q(s,\lambda)$ polynomial given in (13), respectively, and these coefficients depending on MG system parameters are expressed as (27) in Appendix. Substituting the mathematical identities of exponantial term $e^{-j(\omega_c\tau+\phi)}$ and j^{λ} into (15), we can easily obtain the characteristic polynomial in which real and imaginary parts are separated:

$$\begin{aligned} e^{-j(\omega_c\tau+\phi)} &= \cos(\omega_c\tau+\phi) - j\sin(\omega_c\tau+\phi) \\ j^{\lambda} &= \cos\left(\tfrac{\lambda\pi}{2}\right) + j\sin\left(\tfrac{\lambda\pi}{2}\right) \end{aligned} \tag{16}$$

$$\begin{aligned} &\Delta(j\omega_c,\lambda,\tau) = \Re\left(\Delta(j\omega_c,\lambda,\tau)\right) + j\Im\left(\Delta(j\omega_c,\lambda,\tau)\right) = 0 \\ &\Delta(j\omega_c,\lambda,\tau) = K_{PC}A_1(\omega_c) + K_{IC}B_1(\omega_c) + C_1(\omega_c) + j\left[(K_{PC}A_2(\omega_c) + K_{IC}B_2(\omega_c) + C_2(\omega_c)\right] = 0 \end{aligned} \tag{17}$$

Where, $\Re(\bullet)$ and $\Im(\bullet)$ are real and imaginary parts of $\Delta(j\omega_c,\lambda,\tau)$, respectively. Equating both imaginary and real parts of $\Delta(j\omega_c,\lambda,\tau)$ in (17) in which unknowns are (K_{PC} and K_{IC}) to zero, we obtain:

$$\begin{aligned} K_{PC}A_1(\omega_c) + K_{IC}B_1(\omega_c) + C_1(\omega_c) &= 0 \\ K_{PC}A_2(\omega_c) + K_{IC}B_2(\omega_c) + C_2(\omega_c) &= 0 \end{aligned} \tag{18}$$

where the coefficients of $A_i(\omega_c)$, $B_i(\omega_c)$ and $C_i(\omega_c)$ $(i = 1,2)$ polynomials are as follows:

$$\begin{aligned} A_1(\omega_c) &= \left(q'_1\omega_c^{\lambda} - q'_3\omega_c^{\lambda+2}\right)\cos\left(\tfrac{\lambda\pi}{2} - \phi - \tau\omega_c\right) + \left(q'_4\omega_c^{\lambda+3} - q'_2\omega_c^{\lambda+1}\right)\sin\left(\tfrac{\lambda\pi}{2} - \phi - \tau\omega_c\right); \\ B_1(\omega_c) &= (q''_0 - q''_2\omega_c^2)\cos(\tau\omega_c+\phi) + (q''_1\omega_c - q''_3\omega_c^3)\sin(\tau\omega_c+\phi); \\ C_1(\omega_c) &= (p_1 - p_3\omega_c^2 + p_5\omega_c^4)\omega_c^{\lambda}\cos(\lambda\pi/2) + (p_4\omega_c^3 - p_2\omega_c)\omega_c^{\lambda}\sin(\lambda\pi/2); \\ A_2(\omega_c) &= \left(q'_1\omega_c^{\lambda} - q'_3\omega_c^{\lambda+2}\right)\sin\left(\tfrac{\lambda\pi}{2} - \phi - \tau\omega_c\right) + \left(q'_2\omega_c^{\lambda+1} - q'_4\omega_c^{\lambda+3}\right)\cos\left(\tfrac{\lambda\pi}{2} - \phi - \tau\omega_c\right); \\ B_2(\omega_c) &= (q''_2\omega_c^2 - q''_0)\sin(\tau\omega_c+\phi) + (q''_1\omega_c - q''_3\omega_c^3)\cos(\tau\omega_c+\phi); \\ C_2(\omega_c) &= (p_1 - p_3\omega_c^2 + p_5\omega_c^4)\omega_c^{\lambda}\sin(\lambda\pi/2) + (p_2\omega_c - p_4\omega_c^3)\omega_c^{\lambda}\cos(\lambda\pi/2). \end{aligned} \tag{19}$$

Depending on ω_c crossing frequency, we then solve (20) to achieve the stability boundary loci $\ell(K_{PC}, K_{IC}, \omega_c)$ in the (K_{PC}, K_{IC}) $-$space.

$$\begin{aligned} K_{PC} &= \frac{B_1(\omega_c)C_2(\omega_c) - B_2(\omega_c)C_1(\omega_c)}{A_1(\omega_c)B_2(\omega_c) - A_2(\omega_c)B_1(\omega_c)} \\ K_{IC} &= \frac{A_2(\omega_c)C_1(\omega_c) - A_1(\omega_c)C_2(\omega_c)}{A_1(\omega_c)B_2(\omega_c) - A_2(\omega_c)B_1(\omega_c)} \end{aligned} \tag{20}$$

With the help of (18) and (20), complex roots boundaries (CRBs) and real roots boundaries (RRBs) of SBL or stability regions for the MG system are determined. CRBs of stability regions are determined by sweeping the crossing frequency for a range of $\omega_c \in \left[\underline{\omega}_c, \bar{\omega}_c\right]$ in (20). In addition to these stability boundaries, the characteristic equation (13) of MG system has some roots on the origin through $j\omega$-axis. For $\omega_c = 0$, it is clear from (20) that $A_1(0), C_1(0), A_2(0), C_2(0)$ is equal to zero except for $B_1(\omega_c = 0) \neq 0$ and $B_2(\omega_c = 0) \neq 0$. This means that such a crossing through the origin will happen only for $K_{IC} = 0$ [29, 30]. These CRB and RRB loci divide the (K_{PC}, K_{IC}) −plane into unstable and stable regions of the MG system. Sixteen Kharitonov characteristic polynomials represented by $\Delta_n(s, \lambda, \tau)$ $(n = 1, 2, ..., 16)$ in manner of (13) could be concluded for sixteen MG transfer functions given in (12). Although the Kharitonov characteristic polynomials with fractional order are computed due to fractional order degree of integral controller, it is to be noted that the all possible open loop transfer functions of the MG plant is integer order [20, 21]. The procedure mentioned in (14)-(20) is applied to Kharitonov characteristic polynomial corresponding to each of sixteen open loop transfer functions in (12) to identify the all PI controller gains ensuring the stability of relevant open loop transfer function. Consequently, the set of the sixteen stability regions involving the all stabilizing values of PI controller parameters for interval MG system could be computed [20, 21]. Intersecting the sixteen stability regions, the robust stability region containing the robust PI controller gains for the interval MG system is defined as follows:

$$\ell_J(K_{PC}, K_{IC}, \omega_c) = \bigcap_{n=1}^{16} \ell_n(K_{PC}, K_{IC}, \omega_c) \tag{21}$$

Moreover, this study assumes that for the employment of stability boundary locus method, the fractional order degree (λ) of integral controller and communication time delay parameter are fixed in any value, and, thus, these parameters do not have the uncertainty.

4. Results

In the section, the effect of fractional order controller and GPM specifications on robust stability regions for the time-delayed MG having perturbed coefficients is broadly investigated. Then, performance of the obtained robust PI controller gains is investigated under large disturbance events such as load, wind, and solar powers fluctuations. The MG system parameters are taken from [3, 11] and are shown as follows:

$$T_{FC} = 4; K_{FC} = 1; K_{ES} = 1; T_{ES} = 1; K_{MT} = 0.04; M = 10; D = 1; K_{PL} = 1 K_{IL} = 1 \tag{22}$$

Our main purpose is to extract the robust stability region of interval MG having uncertainties. The parametric variations are applied to important parameters such as time constants and gains of FC and ES along with droop characteristic, dampingand inertia of MG system. Upper and lower limits of MG transfer function $G_P(s)$ are computed for parametric uncertainty of $\delta = \pm 15\%$ and the interval transfer function is given as follows:

$$G_P(s) = \frac{\left[\underline{b}_2, \bar{b}_2\right] s^2 + \left[\underline{b}_1, \bar{b}_1\right] s + b_0}{\left[\underline{a}_3, \bar{a}_3\right] s^3 + \left[\underline{a}_2, \bar{a}_2\right] s^2 + \left[\underline{a}_1, \bar{a}_1\right] s + \left[\underline{a}_0, \bar{a}_0\right]} \tag{23}$$

Where upper and lower limits of coefficients in the numerator and denominator of the interval transfer function $G_P(s)$ are calculated as follows:

$$\begin{array}{l} a_0 \in \left[\underline{a}_0, \bar{a}_0\right] = [30.86, 22.29]; a_1 \in \left[\underline{a}_1, \bar{a}_1\right] = [191.8, 106.07]; a_2 \in \left[\underline{a}_2, \bar{a}_2\right] = [227.8, 101.41]; \\ a_3 \in \left[\underline{a}_3, \bar{a}_3\right] = [60.84, 24.57]; b_2 \in \left[\underline{b}_2, \bar{b}_2\right] = [5.29, 2.89]; b_1 \in \left[\underline{b}_1, \bar{b}_1\right] = [5.75, 4.25]; b_0 = 1. \end{array} \tag{24}$$

It should be noted that only $b_0 = 1$ from numerator coefficients is independent of system parameters. The sixteen transfer functions could be established using (23) as stated in (12), and these transfer functions result in Kharitonov characteristic polynomials $\Delta_n(s,\lambda,\tau)$ $(n = 1,2,...,16)$ as represented in (13). The fractional order degree and time delay value of the MG system without GPM specifications $(A = 1, \phi = 0^0)$ are selected as $\lambda = 0.8$ and $\tau = 2s$, respectively. Sweeping the crossing frequency in range of $\omega_c \in [0, 1.1]$, the each stability region corresponding to each Kharitonov characteristic polynomials represented by $\Delta_n(s,\lambda,\tau)$ $(n = 1,2,...,16)$ is computed by SBL method described in (14)-(20). Resulting sixteen stability regions are illustrated in Figure 3. It is inferred from this figure that the boundaries of shaded region constitute the intersection region containing the robust PI controller parameters, ensuring the robustness of the interval MG against the parametric variations.

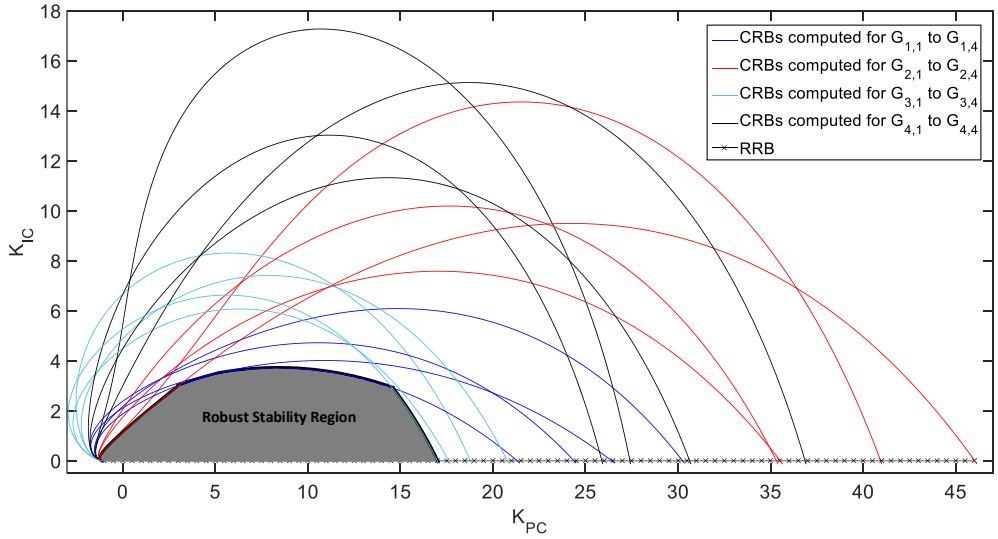

Figure 3. Representation of robust stability region for $\lambda = 0.8$ and $\tau = 2s$.

Moreover, the significant effect of fractional order parameter on the robust stability regions can be observed from Figure 4 where the fractional order value is varied in a range of $\lambda \in [0.6, 1.2]$ for $A = 1, \phi = 0^0$, $\tau = 2s$, uncertainty of $\delta = \pm 15\%$. It is seen from Figure 4 that the robust stability regions for $\lambda < 1$ are larger than the ones for $\lambda \geq 1$. Therefore, it could be concluded that robustness margin of the MG for $\lambda < 1$ considerably expands. The performances of the fractional order based robust PI controller gains presented in Figure 4 are evaluated for $\lambda = 0.6 - 1.2$. In order to examine the robustness on frequency responses of the interval MG, a test scenario including fluctuations of various loads (industrial and residential), wind and solar powers is formed. Multiplying the standard deviations of loads, wind and solar powers given in (7) with the randomly output fluctuations derived using white noise block in MATLAB/Simulink environment [2, 43], the power fluctuations are simulated within $t = 300s$. Figure 5 displays this scenario which shows a large disturbance event by loads and highly penetrated RESs into MG system. These power fluctuations are simultaneously applied to illustrate the effectiveness of robust FOPI controller on frequency responses of the MG system. Figure 6 depicts frequency deviations for $\lambda = 0.6 - 1.2$ when fixed in a PI controller gains $(K_{PC} = 12, K_{IC} = 1.5)$ marked by '*' in Figure 4. It can be observed from Figure 6 that the frequency responses for $\lambda < 1$ exhibit a good dynamic performance and peak overshoots of frequency deviation substantially decrease. Moreover, Figure 6 clearly indicates that the frequency deviations within acceptable ranges are maintained and thus selected PI

controller gains inside robust region provide the robustness of system frequency for the all fractional order of integral controller.

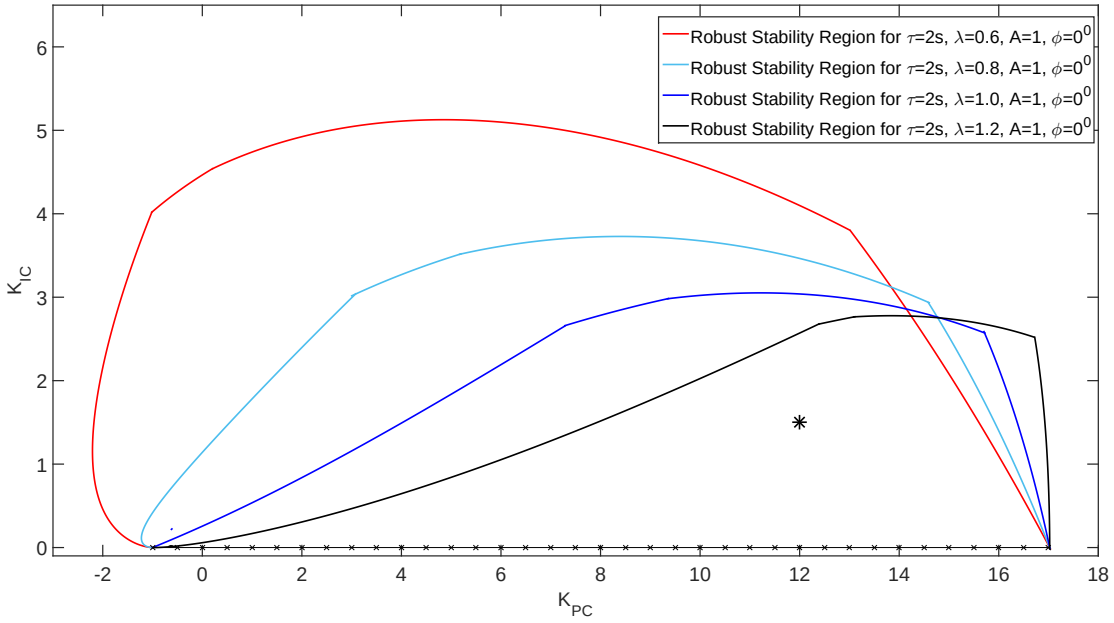

Figure 4. Variation of robustness margins for different fractional order values.

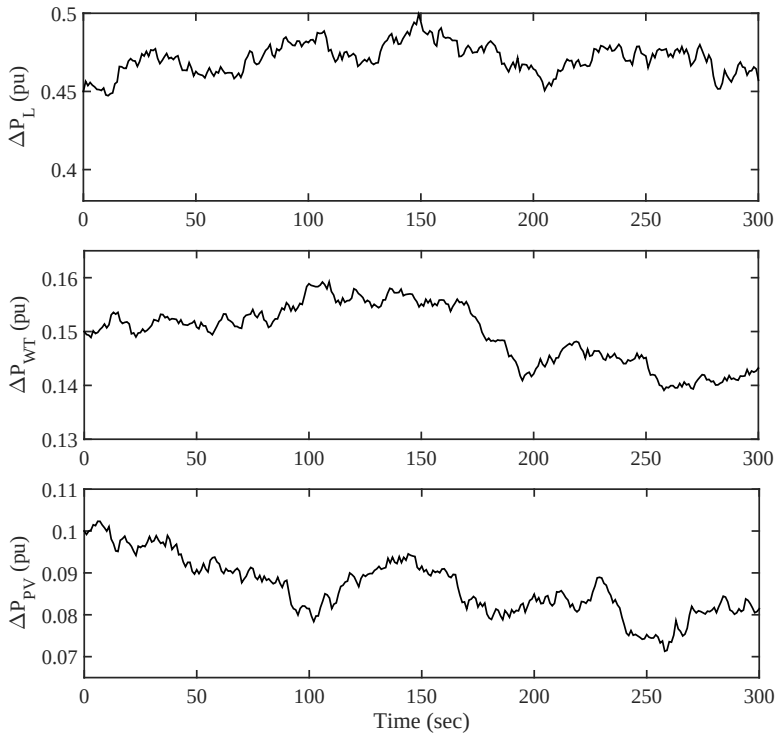

Figure 5. Housing loads, wind and solar power fluctuations.

In order to examine the robust performance ensuring the desired gain and/or phase margins, fractional order degree, the variations in system parameters, the time delay and the crossing frequency range are selected

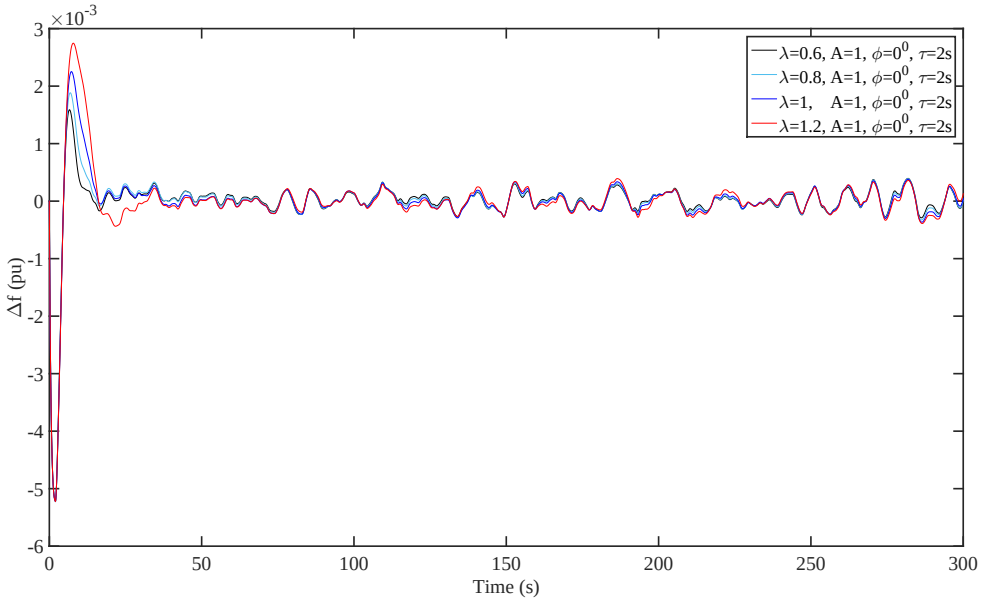

Figure 6. The frequency responses for different fractional order values.

as $\lambda = 0.8$, $\delta = \pm 15\%$, $\tau = 2s$ and $\omega_c \in [0, 1.1]$, respectively. Supposing that desired GPMs are $\phi \geq 20^0$ and $A \geq 1.5$, it can be computed all robust stabilizing K_{PC} and K_{IC} ensuring the stability of each of sixteen Kharitonov transfer functions given in (12). First, the procedure of (13)–(20) is employed to identify the stability regions of Kharitonov transfer functions (12) for specific PM as $\phi = 20^0$ and the intersection of the stability regions is denoted by R1, indicating robust stability region corresponding to desired PM ($\phi = 20^0$) in Figure 7. Similarly, SBL method (13)-(20) is implemented to identify the stability regions of Kharitonov transfer functions for specific GM as $A = 1.5$ and the corresponding robust stability region is depicted by R2 in Figure 7. The shaded intersection of R1 and R2 robust stability regions defines the all robust stabilizing K_{PC} and K_{IC} parameters corresponding to desired GPMs $A \geq 1.5$ and $\phi \geq 20^0$. Finally, the robust stability region not having GPM specification is calculated for $A = 1$ and $\phi = 0^0$ in (13)-(20) and shown by R3 in Figure 7. It should be observed from Figure 7 that the robust regions having desired GPMs are much smaller as compared with robust region R3. The test scenario is simultaneously applied to illustrate the effectiveness of GPM based robust PI controller gains on frequency responses of MG system. Simulation studies for different PI controller gains marked by '*' inside GPMs based robust stability regions in Figure 7 are carried out within $t = 300s$. These robust controller gains are $(K_{PC} = 4, K_{IC} = 1)$ in R1, $(K_{PC} = 4, K_{IC} = 2)$ in R2 and $(K_{PC} = 4, K_{IC} = 3)$ in R3, respectively. In this case, Figure 8 shows the robust frequency responses of the MG for three robust controller parameters. It can be seen from Figure 8 that selected robust PI controller parameters could maintain the frequency stabilization for the studied MG, verifying the robust stability performance of the interval MG. From a practical perspective, Figure 8 indicates that gain and/or phase margin specifications improve settling time and overshoot performance specifications of MG system as compared with dynamical response without GPMs ($A = 1, \phi = 0^0$). Especially, it is observed that the interval MG system is faster for the chosen gains $(K_{PC} = 4, K_{IC} = 1)$ from robust stability region R1 with desired GPMs ($A \geq 1.5$, $\phi \geq 20^0$).

Finally, Figure 9 illustrates the chance of the robust stability regions for parametric uncertainties of $\delta = \pm 5\% - \pm 35\%$. For this, fractional order value, GPM specifications and the time delay are chosen as $\lambda = 0.8$,

$\tau = 2s$ and $A = 1, \phi = 0^0$. Figure 9 illustrates that the set of robust PI controller gains and size of robust stability regions decrease as the system parametric uncertainties increase for $\delta = \pm 5\% - \pm 35\%$.

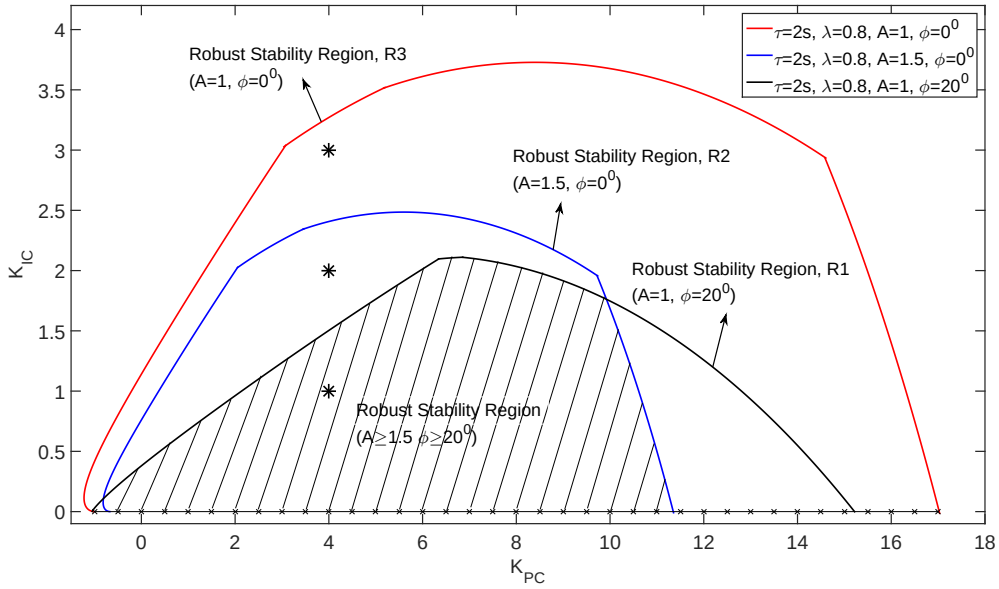

Figure 7. GPMs based robust stability regions for $\lambda = 0.8$ and $\tau = 2s$.

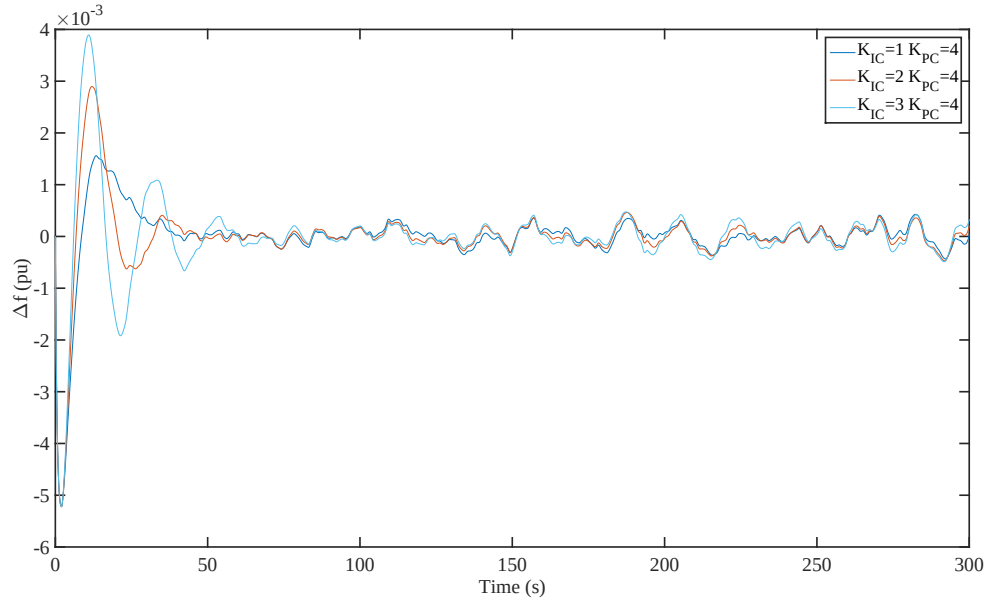

Figure 8. Frequency responses for robust PI parameters.

5. Conclusion

In this paper, the effect of the fractional order of the integral controller and GPMs on robust stability regions of the time-delayed interval MG is broadly studied. In this way, the robust PI controller values guaranteeing robust performance along with robust stability of the interval MG system are computed. It is seen that the order of the integral controller for $\lambda < 1$ increases robust stability regions and thereby substantially enhances the robustness

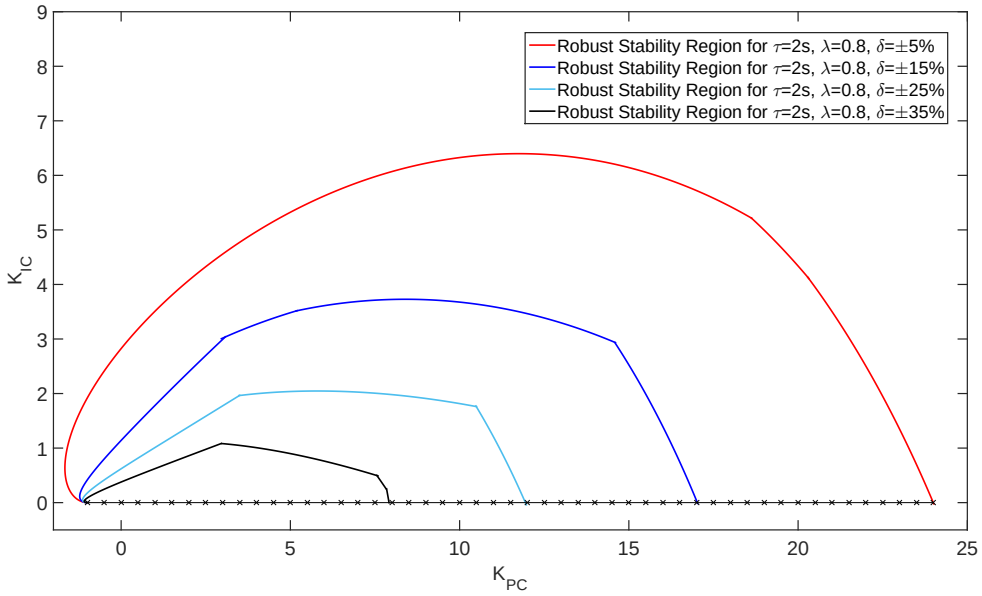

Figure 9. Variations of robust stability regions towards system parametric perturbations.

margin of the MG system. Moreover, it is observed that GPMs based robust performance regions exhibit a good robust performance in terms of damping, settling time, and overshoots. Finally, the effect of parametric uncertainties on the robust regions is investigated. It is observed that robust stability regions decrease with the increase of variations in the system parameters.

In the future, the MG system will enhanced by fuel-cell and electric vehicle (EV) models with secondary control loop. Considering the penetration of RESs and the parametric variations of system, the robust stability regions ensuring the robust controller parameters of the enhanced MG system with communication time delay will be computed to evaluate the robust dynamic behavior and stability of the system.

References

[1] Hatziargyriou N. Microgrids: architecture and control. West Sussex, UK: John Wiley & Sons, 2014.

[2] Li X, Song YJ, Han SB. Frequency control in micro-grid power system combined with electrolyzer system and fuzzy PI controller. Journal of Power Sources 2008; 180: 468-475. doi: 10.1016/j.jpowsour.2008.01.092

[3] Gündüz H, Sonmez Ş, Ayasun S. A comprehensive gain and phase margins-based stability analysis of micro-grid frequency control system with constant communication time delays. IET Generation Transmission and Distribution 2017; 11 (3): 719-729. doi: 10.1049/iet-gtd.2016.0644

[4] Lee DJ, Wang L. Small-Signal Stability Analysis of an Autonomous Hybrid Renewable Energy Power Generation/Energy Storage System Part I: Time-Domain Simulations. IEEE Transactions on Energy Conversion 2008; 23 (1): 311-320. doi: 10.1109/TEC.2007.914309

[5] Lou G, Gu W, Xu Y, Jin W, Du X. Stability Robustness for Secondary Voltage Control in Autonomous Microgrids With Consideration of Communication Delays. IEEE Transactions on Power Systems 2018; 33 (4): 4164-4178. doi: 10.1109/TPWRS.2017.2782243

[6] Bevrani H, Ise T, Miura Y. Virtual synchronous generators: A survey and new perspectives. International Journal of Electrical Power and Energy Systems 2014; 54: 244-254. doi: 10.1016/j.ijepes.2013.07.009

[7] Rapizza MR, Canevese SM. Fast frequency regulation and synthetic inertia in a power system with high penetration of renewable energy sources: Optimal design of the required quantities. Sustainable Energy, Grids and Networks 2020; 24: 100407. doi: 10.1016/j.segan.2020.100407

[8] Kundur P. Power system stability and control. New York, NY, USA: McGraw-Hill, 1994.

[9] Shafiee Q, Guerrero JM, Vasquez JC. Distributed Secondary Control for Islanded MicroGrids - A Novel Approach. IEEE Transactions on Power Electronics 2014; 29 (2): 1018-1031. doi: 10.1109/TPEL.2013.2259506

[10] Ahumada C, Cardenas R, Saez D, Guerrero JM. Secondary control strategies for frequency restoration in islanded microgrids with consideration of communication delays. EEE Transactions on Smart Grid 2016; 7 (3): 1430-1441. doi: 10.1109/TSG.2015.2461190

[11] Mary TJ, Rangarajan P. Delay-dependent Stability Analysis of Microgrid with Constant and Time-varying Communication Delays. Electric Power Components and Systems 2016; 44 (13): 1441-1452. doi: 10.1080/15325008.2016.1170078

[12] Lou G, Gu W, Lu X, Xu Y, Hong H. Distributed Secondary Voltage Control in Islanded Microgrids With Consideration of Communication Network and Time Delays. IEEE Transactions on Smart Grid 2020; 11 (5): 3702-3715. doi: 10.1109/TSG.2020.2979503

[13] Liu S, Wang X, Liu PX. Impact of Communication Delays on Secondary Frequency Control in an Islanded Microgrid. IEEE Transactions on Industrial Electronics 2015; 62 (4): 2021-2030. doi: 10.1109/TIE.2014.2367456

[14] Bevrani H, Feizi MR, Ataee S. Robust frequency control in an islanded microgrid: H∞ and μ -synthesis approaches. IEEE Transactions on Smart Grid 2016; 7 (2): 706-717. doi: 10.1109/TSG.2015.2446984

[15] Khooban MH. Secondary load frequency control of time-delay stand-alone microgrids with electric vehicles. IEEE Transactions on Industrial Electronics 2018; 65 (9): 7416–7422. doi: 10.1109/TIE.2017.2784385

[16] Dehkordi NM, Sadati N, Hamzeh M. Distributed Robust Finite-Time Secondary Voltage and Frequency Control of Islanded Microgrids. IEEE Transactions on Power Systems 2017; 32 (5): 3648-3659. doi: 10.1109/TPWRS.2016.2634085

[17] Veronica AJSJ, Kumar NS, Gonzalez-Longatt F. Robust PI controller design for frequency stabilisation in a hybrid microgrid system considering parameter uncertainties and communication time delay. IET Generation, Transmission and Distribution 2019; 13: 3048 – 3056. doi: 10.1049/iet-gtd.2018.5240

[18] Sharma J, Hote YV, Prasad R. PID controller design for interval load frequency control system with communication time delay. Control Engineering Practice 2019; 89: 154-168. doi: 10.1016/j.conengprac.2019.05.016

[19] Raouf B, Akbarimajd A, Dejamkhooy A, SeyedShenava S. Robust distributed control of reactive power in a hybrid, wind diesel power system with STATCOM. International Transactions on Electrical Energy Systems 2018; 29 (4): 1-18. doi: doi.org/10.1002/etep.2780

[20] Sondhi S, Hote YV. Fractional order PID controller for perturbed load frequency control using Kharitonov's theorem. International Journal of Electrical Power and Energy Systems 2016; 78: 884-896. doi: 10.1016/j.ijepes.2015.11.103

[21] Lamba R, Singla SK, Sondhi S. Design of Fractional Order PID Controller for Load Frequency Control in Perturbed Two Area Interconnected System. Electric Power Components and Systems 2019; 47: 998–1011. doi: 10.1080/15325008.2019.1660736

[22] Sondhi S, Yogesh V, Hote YV. Fractional order PID controller for load frequency control. Energy Conversion and Management 2014; 85: 343-353. doi: 10.1016/j.enconman.2014.05.091

[23] Habibi F, Naghshbandy AH, Bevrani H. Robust voltage controller design for an isolated Microgrid using Kharitonov's theorem and D-stability concept. International Journal of Electrical Power and Energy Systems 2013; 44 (1): 656-665. doi: 10.1016/j.ijepes.2012.08.023

[24] Hao R, Ai Q, Jiang Z, Zhu Y. A novel adaptive control strategy of interconnected microgrids for delay-dependent stability enhancement. Electrical Power and Energy Systems 2018; 99: 566-576. doi: 10.1016/j.ijepes.2018.01.034

[25] Tabak A. Fractional order frequency proportional-integral-derivative control of microgrid consisting of renewable energy sources based on multi-objective grasshopper optimization algorithm. Transactions of the Institute of Measurement and Control 2022; 44 (2): 378–392. doi: 10.1177/01423312211034660

[26] Annamraju A, Bhukya L, Nandiraju S. Robust frequency control in a standalone microgrid: An adaptive fuzzy based fractional order cascade PD-PI approach. Advanced Control for Applications Engineering and Industrial Systems 2021; 3 (3): 566-576. doi: 10.1002/adc2.72

[27] Govindaraju SK, Sivalingam R. Design, analysis, and real-time validation of type-2 fractional order fuzzy PID controller for energy storage–based microgrid frequency regulation. International Transactions on Electrical Energy Systems 2021; 31 (3): e12766. doi: 10.1002/2050-7038.12766

[28] Sahoo G, Sahu RK, Samal NR, Panda S. Analysis of type-2 fuzzy fractional-order PD-PI controller for frequency stabilisation of the micro-grid system with real-time simulation. International Journal of Sustainable Energy 2021; 18: 1-22. doi: 10.1080/14786451.2021.1928131

[29] Tan N, Kaya I, Yeroglu C, Atherton DP. Computation of stabilizing PI and PID controllers using the stability boundary locus. Energy Conversion and Management 2006; 47: 3045-3058. doi: 10.1016/j.enconman.2006.03.022

[30] Hamamcı SE, Tan N. Design of PI controllers for achieving time and frequency domain specifications simultaneously. ISA transactions 2006; 45 (4): 529-543. doi: 10.1016/S0019-0578(07)60230-4

[31] Gündüz H, Sönmez Ş, Ayasun S. The Impact of Electric Vehicles Aggregator on the Stability Region of Micro-Grid System with Communication Time Delay. In: 2019 IEEE Milan PowerTech; Milan, Italy; 2019. pp. 1-6.

[32] Çelik V, Özdemir MT, Bayrak G. The effects on stability region of the fractional-order PI controller for one-area time-delayed load–frequency control systems. Transactions of the Institute of Measurement and Control 2017; 39: 1509-1521. doi: 10.1177/0142331216642839

[33] Sönmez Ş, Ayasun S. Stability region in the parameter space of PI controller for a single-area load frequency control system with time delay. IEEE Transactions on Power Systems 2016; 31 (1): 829-830. doi: 10.1109/TPWRS.2015.2412678

[34] Sönmez Ş. Computation of stability regions for load frequency control systems including incommensurate time delays. Turkish Journal of Electrical Engineering & Computer Sciences 2019; 27: 4596–4607. doi: 10.3906/elk-1904-6

[35] Erol H. Stability analysis of pitch angle control of large wind turbines with fractional order PID controller. Sustainable Energy, Grids and Networks 2021; 26: 100430. doi: 10.1016/j.segan.2021.100430

[36] Özdemir MT. The effects of the FOPI controller and time delay on stability region of the fuel cell microgrid. International Journal of Hydrogen Energy 2020; 45 (60): 35064-35072. doi: 10.1016/j.ijhydene.2020.05.211

[37] Yıldırım B, Khooban MH. Enhancing stability region of time-delayed smart power grids by non-integer controllers. International Journal of Energy Research 2020; 45: 541-553. doi: 10.1002/er.5711

[38] Tan N, Özgüven ÖF, Özyetkin MM. Robust stability analysis of fractional order interval polynomials. ISA Transactions 2009; 48: 166-172. Doi: 10.1016/j.isatra.2009.01.002

[39] Chang CH, Han KW. Gain margins and phase margins for control systems with adjustable parameters. Journal of Guidance, Control, and Dynamics 1990; 13 (3): 404–408. doi: 10.2514/3.25351

[40] Simulink. Simulation and model-based design. Natick, MA, USA: MathWorks, 2019.

[41] Guo J, Liu W, Syed FR, Zhang J. Reliability assessment of a cyber physical microgrid system in island mode. CSEE Journal of Power and Energy Systems 2019; 5 (1): 46-55. doi: 10.17775/CSEEJPES.2017.00770

[42] Jia HJ, Yu XD, Yu Y, Wang C. Power system small-signal stability region with time delay. International Journal of Electrical Power and Energy Systems 2008; 30 (1): 16–22. doi: 10.1016/j.ijepes.2007.06.020

[43] Matsubara M, Fujita G, Shinji T, Sekine T, Akisawa A et al. Supply and Demand Control of Dispersed Type Power Sources in Micro Grid. In: Proceedings of the 13th International Conference on, Intelligent Systems Application to Power Systems; Arlington, VA, USA; 2005. pp. 67-72.

Appendix

Coefficients of numerator and denominator expressed in (9) are as follows:

$$\begin{array}{l} a_0 = (D + K_{ES} - K_{FC} + 1/K_{MT}); a_1 = (T_{ES} + T_{FC})(D + 1/K_{MT}) + M + K_{ES}T_{FC} - K_{FC}T_{ES}; \\ a_2 = MT_{ES} + MT_{FC} + T_{ES}T_{FC}(D + 1/K_{MT}); a_3 = MT_{ES}T_{FC}; b_0 = 1; \\ b_1 = T_{ES} + T_{FC}; b_2 = T_{ES}T_{FC}. \end{array} \tag{25}$$

Upper and lower limits of numerator and denominator expressed in (10) and (11) are:

$$\begin{array}{l} \bar{a}_3 = \bar{M}\bar{T}_{ES}\bar{T}_{FC}; \underline{a}_3 = \underline{MT}_{ES}\underline{T}_{FC}; \bar{a}_2 = \bar{M}\bar{T}_{ES} + \bar{M}\bar{T}_{FC} + \bar{T}_{ES}\bar{T}_{FC}\left(\bar{D} + 1/_{MT}\right); \\ \underline{a}_2 = \underline{MT}_{ES} + \underline{MT}_{FC} + \underline{T}_{ES}\underline{T}_{FC}\left(\underline{D} + 1/\bar{K}_{MT}\right); \\ \bar{a}_1 = \left(\bar{T}_{ES} + \bar{T}_{FC}\right)\left(\bar{D} + 1/\underline{K}_{MT}\right) + \bar{M} + \bar{K}_{ES}\bar{T}_{FC} - \underline{K}_{FC}\underline{T}_{ES}; \\ \underline{a}_1 = \left(\underline{T}_{ES} + \underline{T}_{FC}\right)\left(\underline{D} + 1/\bar{K}_{MT}\right) + \underline{M} + \underline{K}_{ES}\underline{T}_{FC} - \bar{K}_{FC}\bar{T}_{ES}; \bar{a}_0 = \left(\bar{D} + \bar{K}_{ES} - \underline{K}_{FC} + 1/\underline{K}_{MT}\right); \\ \underline{a}_0 = \left(\underline{D} + \underline{K}_{ES} - \bar{K}_{FC} + 1/\bar{K}_{MT}\right); \bar{b}_2 = \bar{T}_{ES}\bar{T}_{FC}; \underline{b}_2 = \underline{T}_{ES}\underline{T}_{FC}; \bar{b}_1 = \bar{T}_{ES} + \bar{T}_{FC}; \\ \underline{b}_1 = \underline{T}_{ES} + \underline{T}_{FC}; b_0 = 1. \end{array} \tag{26}$$

The coeefficients of the caharacteristic equation obtained in (14) are as follows:

$$\begin{array}{l} p_5 = (a_3 + K_{PL}Mb_2); p_4 = (a_2 + DK_{PL}b_2 + K_{IL}Mb_2 + K_{PL}Mb_1); \\ p_3 = (a_1 + DK_{IL}b_2 + DK_{PL}b_1 + K_{IL}Mb_1 + K_{PL}Mb_0); \\ p_2 = (a_0 + DK_{IL}b_1 + DK_{PL}b_0 + K_{IL}Mb_0); \\ p_1 = (DK_{IL}b_0); q_4 = AK_{PC}K_{PL}b_2; q_3 = AK_{PC}(K_{IL}b_2 + K_{PL}b_1) + AK_{IC}K_{PL}b_2; \\ q_2 = AK_{IC}(K_{IL}b_2 + K_{PL}b_1) + AK_{PC}(K_{IL}b_1 + K_{PL}b_0); \\ q_1 = AK_{IC}(K_{IL}b_1 + K_{PL}b_0) + AK_{PC}K_{IL}b_0; q_0 = AK_{IC}K_{IL}b_0; \\ q'_4 = q''_3 = AK_{PL}b_2; q'_3 = q''_2 = A(K_{IL}b_2 + K_{PL}b_1); \\ q'_2 = q''_1 = A(K_{IL}b_1 + K_{PL}b_0); q'_1 = q''_0 = AK_{IL}b_0. \end{array} \tag{27}$$